Green Chemistry

Fabrication of Reusable Bifunctional Biomimetic Ti^{4+}-Phosphorylated Cellulose Monolith with Coral-Like Structure for Enrichment of Phosphorylated and Glycosylated Peptides

Journal:	*Green Chemistry*
Manuscript ID	GC-ART-06-2021-002206.R1
Article Type:	Paper
Date Submitted by the Author:	06-Aug-2021
Complete List of Authors:	Zhang, Luwei; Department of Applied Chemistry, Graduate School of Engineering, Osaka University, Graduate School of Engineering Osaka University Wang, Yan; Osaka University, Pan, Lei; Dalian Institute of Chemical Physics Tang, Ruizhi; Dalian Institute of Chemical Physics Asoh, Taka-Aki; Osaka University, Applied Chemistry Ou, Junjie; Dalian Institute of Chemical Physics, Uyama, Hiroshi; Osaka Univerisity,

ARTICLE

Fabrication of Reusable Bifunctional Biomimetic Ti^{4+}-Phosphorylated Cellulose Monolith with Coral-Like Structure for Enrichment of Phosphorylated and Glycosylated Peptides

Received 00th January 20xx,
Accepted 00th January 20xx

DOI: 10.1039/x0xx00000x

Luwei Zhang[a], Yan Wang[a], Lei Pan[b], Ruizhi Tang[b], Taka-Aki Asoh*[a], Junjie Ou[b], and Hiroshi Uyama*[a]

Protein phosphorylation and glycosylation, as two of the most important post-translational modifications of proteins, are of great significance to humans. The development of materials that can selectively enrich phosphopeptides and glycopeptides from complex biological samples has considerable meaning. In this work, a environmentally friendly bionic cellulose-derived monolithic material (TiPCM) with a coral-like structure was prepared using a thermally induced phase separation (TIPS) method, which exhibited good hydrophilicity, a satisfactorily porous structure, and a large quantity of titanium ions allowing it to simultaneously enrich both phosphopeptides and glycopeptides or enrich phosphopeptides alone from biological samples. The prepared TiPCM materials could enrich phosphopeptides and glycopeptides, respectively, from a BSA/β-casein (molar ratio, 5000/1) and BSA/IgG (molar ratio, 1000/1) mixtures demonstrating that it had excellent selectivity for phosphopeptides and glycopeptides. Meanwhile, it is worth mentioning that TiPCM materials possess reusability in the enrichment of phosphopeptides, which has not been studied much in literature. Moreover, three replicate analyses from 200 μg tryptic digest of milk identified 119 unique phosphopeptides from 38 phosphoproteins, while identifying 180 glycopeptides from 93 unique glycoproteins and their corresponding 148 independent glycosylation sites. These results demonstrate the potential of TiPCM materials in the analysis of phosphorylated and glycosylated proteomics.

Introduction

The post-translational modifications (PTMs) of proteins refer to processes such as the chemical modification and side-chain processing of protein precursors, which endow various life functions to proteins. Among more than 300 known PTMs, protein phosphorylation and glycosylation are considered to be the two most important and widely studied. Almost all cellular activities are regulated by phosphorylation.[1-4] Abnormal protein phosphorylation has been found to be closely related to more than 400 diseases, including cancer and diabetes.[5-9] Studying protein phosphorylation can provide important information for identifying cancer markers, discovering drug targets, *etc*. Similarly, more than 50% of human proteins can be modified through glycosylation, the polysaccharide chains attached to glycosylated proteins being involved in a variety of important life processes.[10, 11] Generally, aberrant protein glycosylation is closely associated with many cancers, neurological diseases, and Alzheimer's.[12-15] Moreover, studies on the novel coronavirus disease (COVID-2019) has shown that glycosylated proteins on the surface of coronaviruses play a crucial role. When they invade cells, these glycosylated proteins also being major targets of antibodies.[16, 17] Thus far, most of the identified disease markers are glycosylated proteins.[18, 19] Consequently, the study of protein phosphorylation and glycosylation is of great importance.

A current analytical method commonly used to explore protein phosphorylation and glycosylation is to digest proteins into peptides and then to analyze them using mass spectrometry (MS). However, due to the low abundance of phosphorylated and glycosylated peptides in protein digestion, a large number of non-phosphopeptide and non-glycopeptide signals interfere with the phosphopeptide and glycopeptide signals, making it difficult to analyze protein digestion samples directly using MS. Consequently, the development of enrichment methods with specificity is of great importance for the analysis of protein phosphorylation and glycosylation. Currently, phosphopeptide enrichment methods include metal oxide affinity chromatography (MOAC), immobilized metal affinity chromatography (IMAC), immunoaffinity chromatography (IAC) and so on.[20-23] Among these methods, IMAC is the most widely used in phosphopeptide enrichment due to its high specificity and low steric effects, which are achieved by the chelation and static adsorption between phosphate groups in phosphopeptides and metal ions.[24] Moreover, some strategies—including lectin affinity chromatography, hydrazine

[a] *Department of Applied Chemistry, Graduate School of Engineering, Osaka University, Suita 565-0871, Japan*
[b] *CAS Key Laboratory of Separation Science for Analytical Chemistry, Dalian Institute of Chemical Physics, Chinese Academy of Sciences, Dalian, 116023, China*

chemistry, boric acid chemistry, and hydrophilic interaction chromatography (HILIC)—have been commonly applied to glycopeptide enrichment.[25, 26] Of these strategies, HILIC exhibits many advantages, such as its ability to enrich various glycosylated peptides, retaining intact oligosaccharide chain information. Compared to non-glycopeptides, glycopeptides with saccharide chains exhibit stronger hydrophilicity which can be selectively enriched by hydrophilic materials. The materials that have been used in glycopeptide enrichment have been widely reported.[27] However, there are disadvantages, namely their complicated and environmentally unfriendly preparation processes and high cost. Most importantly, there are few reports of materials that can simultaneously enrich both phosphopeptides and glycopeptides, although various materials used in phosphopeptide and glycopeptide enrichment processes have been extensively reported.

Conversely, some corals—as one of the oldest marine organisms on Earth—have evolved a unique dendritic structure which allows them to efficiently capture food from flowing seawater. Their predatory behavior is very similar to that of IMAC and HILIC materials in capturing phosphopeptides and glycopeptides from a loading solution. Consequently, the dendritic coral-like structure can increase permeability to improve the mass transfer rate between the material and the enrichment solution, reducing the steric effect between the peptides and the material during enrichment. Moreover, the microstructure that exists in dendritic surfaces is beneficial in providing more sites for the material to adsorb phosphopeptides and glycopeptides.

Inspired by coral, we fabricated a Ti^{4+}-phosphorylated cellulose monolith (TiPCM) with a coral-like structure for the enrichment of phosphorylated and glycosylated peptides in this study. Cellulose is considered to be the most promising, sustainable, and renewable carbon source as it is one of the most widely distributed and abundant polysaccharides in nature.[28] It has the advantages of being environmentally friendly, non-toxic, inexpensive, and widely available. In recent years, our group fabricated a cellulose monolith (CM) with a coral-like structure by changing its preparation conditions.[29-32] We prepared phosphorylated CM *via* an esterification reaction, after which the titanium ion (Ti^{4+}) was modified on the surface of its skeleton *via* chelation between the Ti^{4+} and the phosphate group. A large number of phosphate groups on the surface of the TiPCM clearly advanced the hydrophilicity of the CM, offering many sites to chelate Ti^{4+}. Most importantly, the entire process is green, placid, and simple, the resulting TiPCM exhibiting satisfactory performance in the analysis of protein phosphorylation and glycosylation.

Experimental

Chemicals and materials

Cellulose acetate (CA, L30) with an acetylation degree of 55% was provided by Daicel Co., Ltd. Japan. Sodium dihydrogen phosphate (NaH_2PO_4), sodium hydrogen phosphate (Na_2HPO_4), sodium hydroxide, urea, ammonium bicarbonate, ammonia water, and acetonitrile (ACN) were purchased from FUJIFILM Wako Pure Chemical Corporation, Japan. Dithiothreitol (DTT), Iodoacetamide (IAA), β-casein, immunoglobulin G (IgG), bovine albumin (BSA), trypsin, and trifluoroacetic acid (TFA) were purchased from Sigma Co., Ltd. USA. Titanium (IV) sulfate solution was purchased from Kishida Chemical Co., Ltd. Japan. Deionized water was doubly distilled and purified using the Milli-Q system (Millipore Inc., Milford, MA, USA).

Preparation of the cellulose monolith (CM)

The preparation process of the CM was described in our previous report.[31] In brief, a certain amount of CA was dissolved in dimethylformamide (DMF) at 90 °C. Then, 1-hexanol was added dropwise into the solution whilst it was stirred. The solution was placed into a water bath at 20 °C for 24 h to achieve phase separation after it had become transparent. Subsequently, the product was washed three times using ethanol before being dried under vacuum to obtain the CA monolith. The resulting CA monolith was hydrolyzed using 0.5 mol L^{-1} NaOH aqueous solution, and then washed with deionized water and dried under vacuum to obtain the CM.

Preparation of the Ti^{4+}-phosphorylated CM (TiPCM)

As shown in **Scheme 1a**, the 40 mL aqueous solution containing urea (18.7 g), Na_2HPO_3 (11.1 g), and NaH_2PO_3 (24.9 g) was circulated through the prepared CM for 1 h using a pump. The CM filled with the aqueous solution was heated in an oven at 140 °C overnight, and then washed with water and dried to obtain the phosphorylated cellulose monolithic (PCM) material. Subsequently, the titanium phosphate solution was passed through the PCM for 4 h using a pump to achieve the incorporation of Ti^{4+} and the PCM. The product was washed using deionized water, and then dried under vacuum to acquire the TiPCM.

Instruments and methods

Attenuated total reflection Fourier transform infrared (ATR-FTIR) spectroscopy (Thermo Scientific Nicolet iS 5) was used to confirm the synthesis of the CM and PCM. The pore structure and morphology of the materials were examined by means of scanning electron microscopy (SEM, Hitachi S-3000N, Tokyo, Japan). The thermal stability of the materials was confirmed through thermogravimetric analysis (TGA, Hitachi TG/DTA7200, Tokyo, Japan). The hydrophilicity of the materials was evaluated by means of the water contact angle obtained using a Drop Master DM300 (Kyowa Interface Science, Japan) with 1.0 μL water drops. The Brunauer-Emmett-Teller (BET) surface area of the materials was evaluated by using a nitrogen adsorption–desorption analyzer (Quantachrome Instruments, USA). X-ray photoelectron spectroscopy (XPS, JEOL JPS-9010MC) was employed to investigate the surface chemistry of the materials, using monochromatized Al-Kα radiation (1486.6 eV). The XPS spectra were determined at fixed analyzer pass energies of 160 eV and 10 eV, respectively. The binding energies were referred to as C-H (sp^3) carbon for the C 1s peak set at 284.8 eV.

Denaturation and enzymatic digestion of protein solutions

One militer of denaturing solution containing 8.0 mol · L^{-1} urea and 0.1 mol · L^{-1} ammonium bicarbonate was used to dissolve 2 mg BSA/IgG/β-casein/milk specimens, followed by the addition of 20 mmol · L^{-1} DTT solution. The mixture was incubated at

Scheme 1 (a) Preparation of the TiPCM. (b) Workflow of the simultaneous enrichment of phosphopeptides and glycopeptides. (c) Workflow of the individual enrichment of phosphopeptides. Buffer 1: 79% ACN + 3% TFA + 18% H_2O, Buffer 2: 50% ACN + 3% TFA + 47% H_2O.

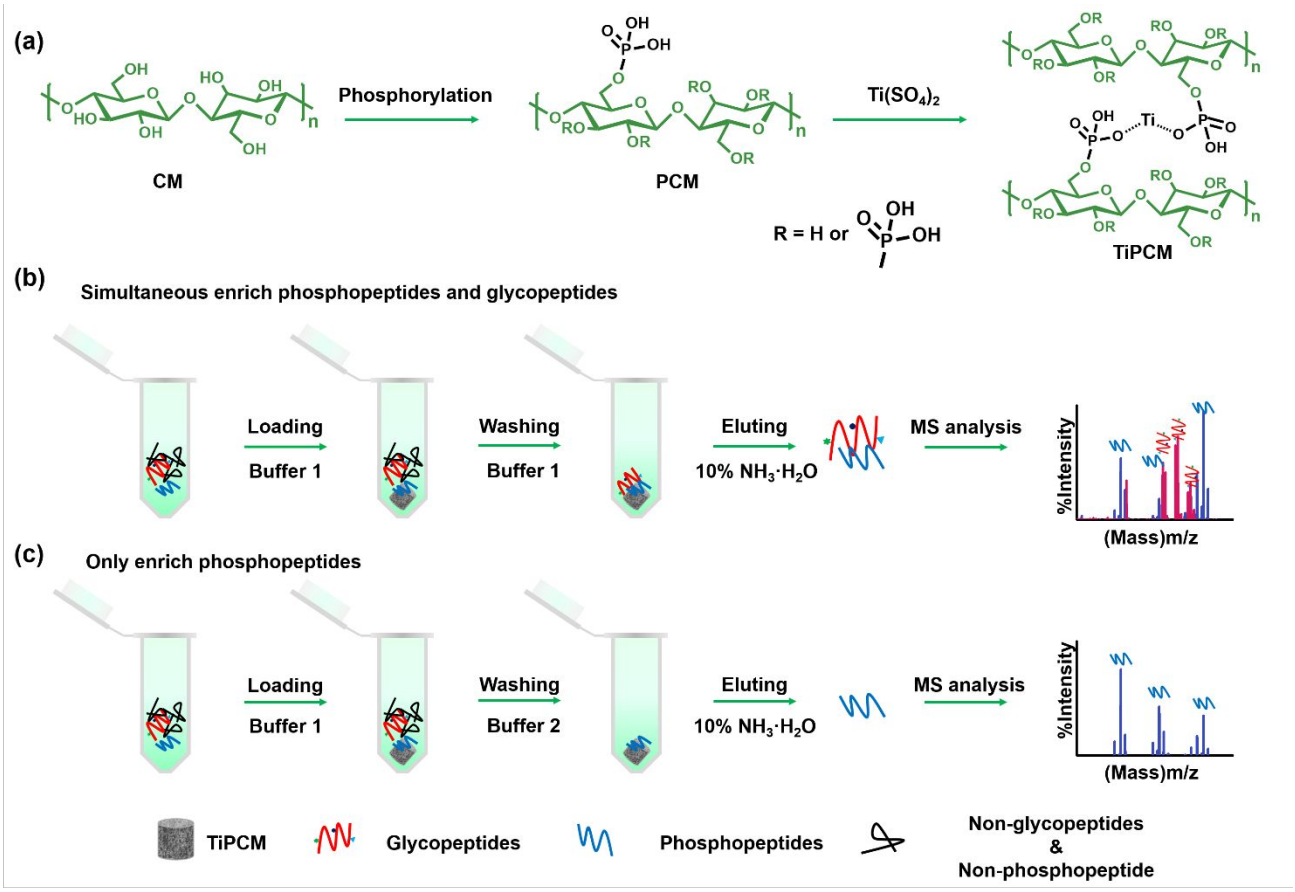

60 °C for 1 h, after which it was incubated further for 30 min in the dark at room temperature after IAA (7.4 mg) was added. The ammonium bicarbonate solution (0.1 mol·L^{-1}) was used to dilute the mixture 8 times, and 80 μg of trypsin was added for the BSA/IgG/β-casein/milk specimens to incubate at 37 °C for 16 h. Subsequently, a 10% TFA aqueous solution was adapted to adjust the pH of the mixture to approximately 2–3. A custom C18 column was selected to perform solid phase extraction (SPE). The eluted peptide solution was dried under vacuum and dissolved in a 0.1% FA (2.0 mL) aqueous solution. Eventually, the resulting peptide solution was dispensed and dried using a freeze dryer, followed by storage at −20 °C.

Enrichment of phosphopeptides and glycopeptides

The process of enrichment of phosphopeptides and glycopeptides usually includes loading, washing and elution, as shown in **Scheme 1**. For simultaneous enrichment of phosphopeptides and glycopeptides, as shown in **Scheme 1b**. The loading solution (100 μL × 3, Buffer 1, ACN/H_2O/TFA = 79/18/3, v/v/v) was used in washing a certain amount of the TiPCM 3 times, and then the loading solution (100 μL, Buffer 1, ACN/H_2O/TFA = 79/18/3, v/v/v) with a certain amount of BSA/IgG/β-casein tryptic digest was added. A bio shaker was employed to incubate the mixture at 25 °C for 0.5 h. Subsequently, the mixture was centrifugated at 5,000 g for 2 min to remove solution, and washing solution (100 μL × 3, Buffer 1, ACN/H_2O/TFA = 79/18/3, v/v/v) was used in washing the residual substance for 15 min 3 times. The elution solution (50 μL × 2, 10% $NH_3 \cdot H_2O$) was adopted in eluting the captured glycopeptides for 10 min at 25 °C twice. Finally, MALDI-TOF was employed to analyze the eluted solution.

Conversely, **Scheme 1c** shows the process of enriching only phosphopeptieds. A certain amount of the TiPCM was washed with loading solution (100 μL × 3, Buffer 1, ACN/H_2O/TFA = 79/18/3, v/v/v) 3 times. Then, loading solution (100 μL, Buffer 1, ACN/H_2O/TFA = 79/18/3, v/v/v) with a certain amount of BSA/IgG/β-casein tryptic digest was added to load sample. enriching process of only enriching phosphopeptieds is similar with simultaneous enrichment of phosphopeptides and glycopeptides except for wasing solution. For only enriching phosphopeptieds, Buffer 2 (ACN/H_2O/TFA = 50/47/3, v/v/v) was chosen as washing solution.

To enrich the phosphopeptides and glycopeptides from complex sample, a certain amount of the TiPCM was washed with loading solution (100 μL × 3, Buffer 1, ACN/H_2O/TFA = 79/18/3, v/v/v), and then 200 μg tryptic digest of milk dissoved in 500 μL Buffer 1 was added to load sample. A bio shaker was employed to incubate the mixture at 25 °C for 0.5 h. Subeseuqently, the mixture was centrifugated at 5,000 g for 2 min to remove solution, and washing solution (500 μL × 3, Buffer 1, ACN/H2O/TFA = 79/18/3, v/v/v) was used in washing the TiPCM for 15 min 3 times. The elution solution (50 μL × 2, 10% $NH_3 \cdot H_2O$) was adopted in eluting the captured phosphopeptides and glycopeptides for 10 min at 25 °C twice. Finally, the glycopeptide solutions from the two elution solutions were mixed, lyophilized, deglycosylated, and analyzed by liquid-chromatography–mass-spectrometry (LC-MS). The LC-

MS experiments are detailed in the Supporting Information section.

Results and discussion

Preparation of the TiPCM

Corals, as one of the oldest marine organisms on Earth, possess unique dendritic structures which allow them to efficiently use flowing seawater to capture food. Inspired by their unique structure, a monolithic material (TiPCM) with a coral-like structure was fabricated to apply in the field of phosphopeptide and glycopeptide enrichment in this work. The unique coral-like structure in the TiPCM facilitates the reduction of steric effects between the peptide and the material during enrichment and provides more sites to adsorb peptides. As previously reported, our group discovered that the skeleton of the CM could be changed by adjusting the CA concentration.[31] As shown in **Figure S1**, when the CA concentrations were 80 and 100 mg · mL^{-1}, respectively, the prepared CM-1 and CM-2 specimens exhibited a dendritic coral-like structure on which many villi exist. As the CA concentrations increased to 120 mg · mL^{-1}, the CM-3 skeleton changed to a network structure as shown in **Figures S1c** and **S1f**. It can be seen from **Table 1**, that the CM-1 exhibited excellent permeability (3.07×10^{-12} m^2) when the CA concentration was 80 mg · mL^{-1}. Consequently, the CM-1 was chosen for the preparation of the TiPCM in the subsequent experiments.

Table 1 Detailed composition for fabrication of the CM.

Monolith	DMF (mL)	1-Hexanol (mL)	CA concentration (mg·mL^{-1})	Permeability ($\times 10^{-12}$ m^2)
CM-1	10	15	80	3.07
CM-2	10	15	100	0.12
CM-3	10	15	120	0.01

Physical properties of the TiPCM

To explore whether the skeleton of the material could successfully mimic the structure of coral, SEM was used to observe the microscopic morphology of the CM, PCM and TiPCM. As shown in **Figures 1a**[33]**, 1b, 1e,** and **1f**, the prepared CM material had the dendritic skeleton structure of coral. After magnified observation, the surface of the dendritic structure could be seen to have a fluff-like structure similar to the surface of the dendritic structure in coral. After phosphorylation and chelation, both the PCM and TiPCM maintained the coral-like skeleton structure of the CM. The coral-like structure still had a rough surface, but the fluff-like structure on the surface of the coral-like structure had been destroyed, which may have been due to the destruction of cellulose crystals by urea during the phosphorylation process (**Figures 1c, 1d, 1g,** and **1h**).

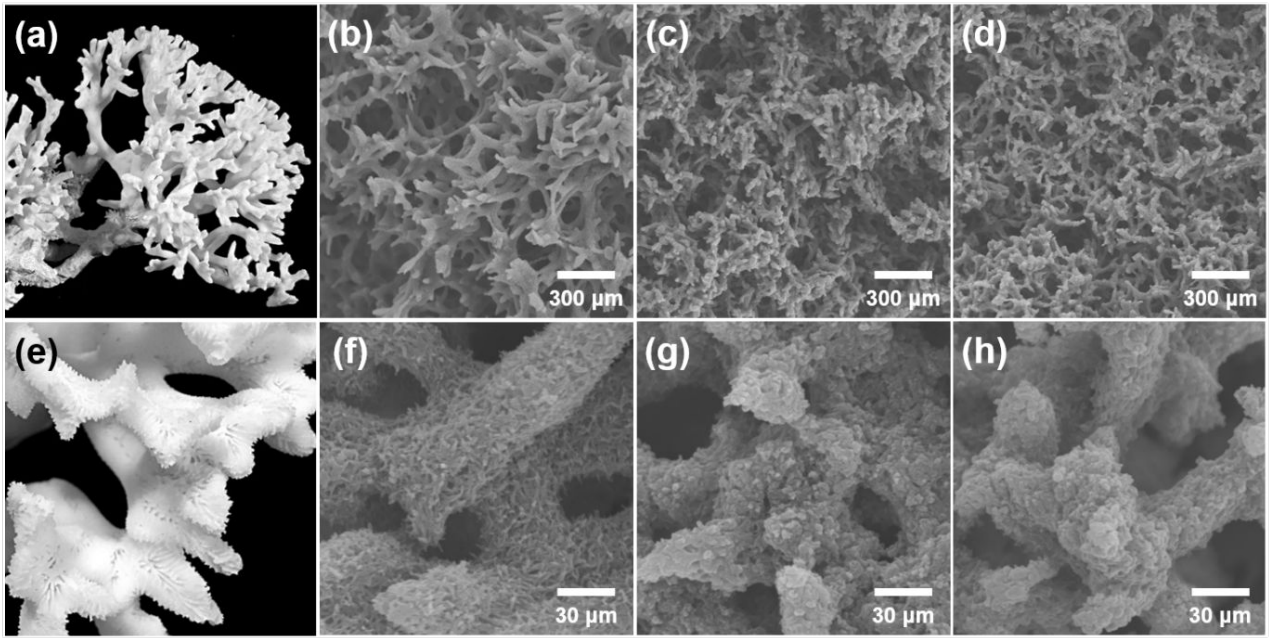

Figure 1 (a, e) Photograph of *Paraclavarina*, a type of coral that lives in Australia.[33] SEM images of (b, f) the CM, (c, g) PCM, and (d, h) TiPCM (at 500×, 5000×, 500×, 5000×, 500×, and 5000× magnification, respectively).

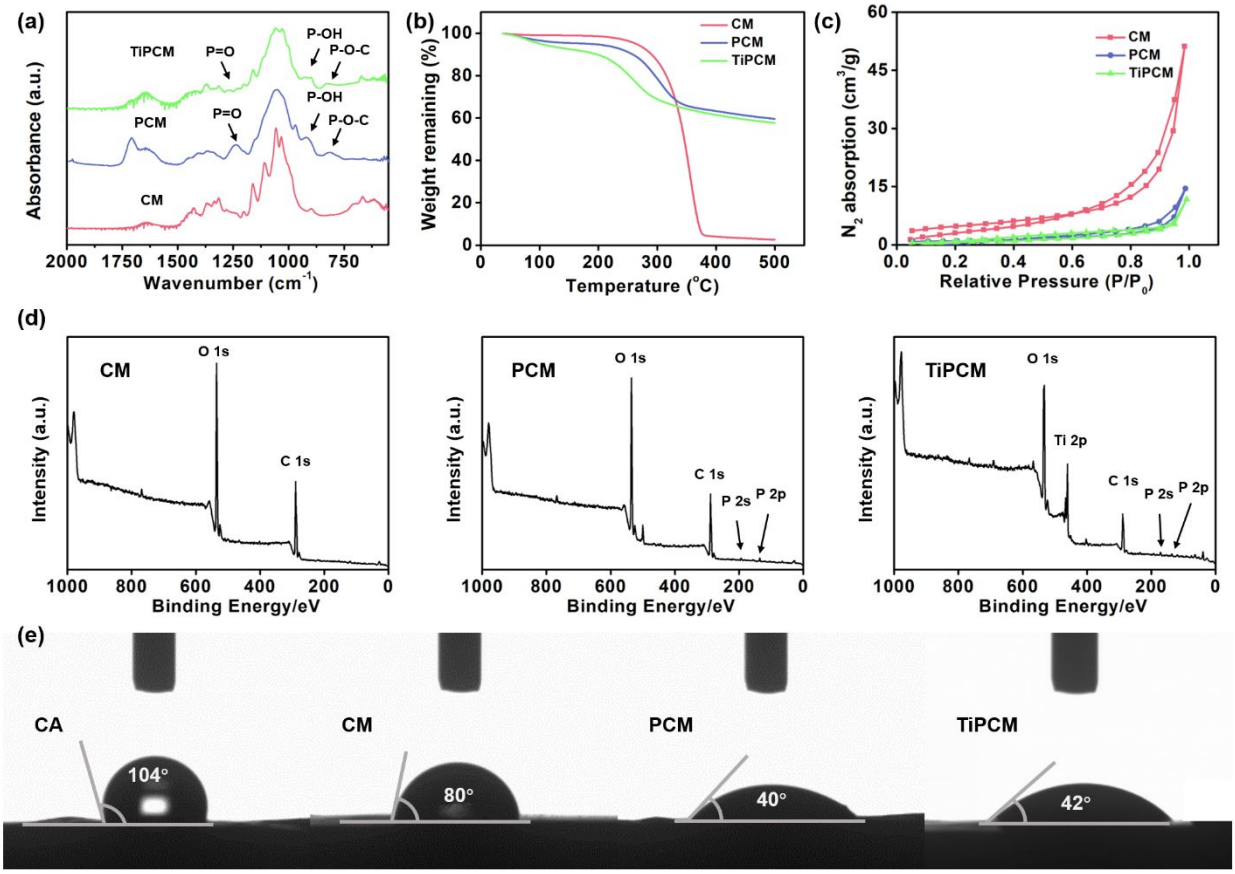

Figure 2 (a) ATR-FTIR spectra, (b) thermogravimetric curve at a heating rate of 10 °C·min^{-1} within a nitrogen atmosphere, (c) nitrogen adsorption-desorption isotherms, (d) XPS spectra of the CM, PCM and TiPCM and (e) the water contact angle of CA, CM, PCM, and TiPCM.

Furthermore, the CM, PCM and TiPCM materials were characterized by ATR-FTIR to verify if the phosphorylation of cellulose had been successful. As seen in **Figure 2a**, when compared with the spectrum of the CM, the signals appeared at 1,232 (P=O), 924 (P-OH), and 827 cm^{-1} (P-O-P) which were assigned to be the characteristic peaks of the phosphate group in the PCM and TiPCM. This result demonstrated that the CM had been successfully phosphorylated into the PCM, and that the phosphate group still existed in the TiPCM.

The thermal stability of the materials was evaluated by TGA. As shown in **Figure 2b**, the CM, PCM, and TiPCM exhibited good stability before 200 °C. Among the three materials, the CM showed the best thermal stability because there was no obvious weight loss until 250 °C. By contrast, obvious weight loss of the PCM and TiPCM were found in the range of 200–300 °C (**Figure 2b**). It is worth mentioning that the remaining weight of the CM approached zero above 400 °C, while the weight of the PCM and TiPCM were 59.6% and 57.7%, respectively. Because high temperature will lead to hydrolysis of ester groups and release the phosphoric acid on the surface of cellulose. The phosphoric acid as a catalyst for the dehydration of cellulose chains, charring the surface and leading to the formation of a thermally resistant coating capable of protecting the remaining internal material at over 400 °C.[34] The above results showed that phosphate groups had been successfully introduced to the CM. Moreover, the specific surface area of these materials was examined by measuring the nitrogen adsorption/desorption isotherm. As shown in **Figure 2c,** the BET specific surface area of the CM was 16.7 $m^2 \cdot g^{-1}$. However, after phosphorylation, the specific surface area of the PCM and TiPCM decreased to 3.3 and 2.9 $m^2 \cdot g^{-1}$, respectively. This phenomenon was possibly caused by the destruction of cellulose crystals, the addition of urea leading to the collapse of mesopores in the CM which was consistent with the SEM images (**Figure 1**). The XPS spectra was utilized to confirm the introduction of Ti^{4+} onto the surface of the PCM. It could be seen from the spectrum of the CM (**Figure 2d**) that the signals at 535.11 and 288.88 eV, respectively, corresponded to O 1s and C 1s. As for the PCM, the peaks of P 2s and P 2p also appeared at 193.96 and 136.07 eV (**Figure 2d**) except for the peaks of O 1s at 535.04 eV and C 1s at 288.95 eV, demonstrating that the phosphate groups had been modified on the surface of the PCM. Furthermore, the peaks of Ti 2p could be seen at 461.01 eV (**Figure 2d**), proving that the Ti^{4+} successfully chelated with the phosphate groups in the TiPCM. In addition, the hydrophilicity of the material showed a strong influence on the enrichment of the glycosylated peptides. The water contact angle technique was employed to examine the hydrophilicity of the materials. To avoid the effects of surface roughness and porous structure, the CA monolith, CM, PCM, and TiPCM were compressed to smooth sheets to determine their hydrophilicity. As shown in Figure 2e, the water contact angle of the CA monolith was 104°, indicating that it was a

hydrophobic material because of the presence of many ester groups on its surface. Compared with the CA monolith, the water contact angle of the CM decreased to 80°, exhibiting hydrophilicity as the ester groups had been hydrolyzed by NaOH to hydroxyl groups. After the CM was phosphorylated, the hydrophilicity of the PCM and TiPCM was significantly strengthened, and their water contact angles diminished to 40° and 42°, respectively. The phenomenon demonstrated that a large number of hydrophilic phosphate groups had been introduced onto the surface of the CM, and phosphorylation had succeeded. As a result, the TiPCM exhibited good hydrophilicity and has the potential to enrich glycopeptides.

Enrichment of phosphopeptides and glycopeptides

The content of the organic phase in the loading buffer is an important factor for the enrichment of peptides.[35] As for phosphopeptides and glycopeptides, their retention behavior on the surface of the materials was significantly influenced by the content of the organic solvent. To enrich glycopeptides and phosphopeptides simultaneously, the effect of different ACN concentrations in the loading buffer was examined, as shown in **Figure S2**. When ACN/H_2O/TFA (83/14/3, v/v/v) was used as the loading solution, a high non-phosphopeptide signal intensity was observed in **Figure S2a**, and strong non-glycopeptide signals could be observed in **Figure S2e**. As the ACN content decreased to 81%, the non-phosphopeptide signal intensity decreased (**Figure S2b**) but was not weak, and the number of non-glycopeptides was reduced (**Figure S2f**). When ACN/H_2O/TFA (79/18/3, v/v/v) was selected as the loading solution, the number of non-phosphopeptides diminished, and the phosphopeptide signals could be clearly seen, as shown in **Figure S2c**. Moreover, the glycopeptide signals were prominent (**Figure S2g)**. However, when the organic phase further decreased to ACN/H_2O/TFA (77/20/3, v/v/v), the enrichment performance for phosphopeptides (**Figure S2d**) was not perceptibly different from the ACN/H_2O/TFA (79/18/3, v/v/v) case (**Figure S2c**). With regard to the glycopeptide enrichment results, the non-glycopeptide signals virtually completely disappeared, the glycopeptides becoming weak at the same time as observed in **Figure S2h**. Consequently, ACN/H_2O/TFA (79/18/3, v/v/v) was chosen to be the loading solution in the subsequent experiments.

The TFA content in the enrichment solution system also effects the retention behavior of glycopeptides and phosphopeptides. To further optimize the enrichment conditions of the two kinds of peptides, different TFA content (1%, 3%, and 5%, v/v) in the loading and washing solutions was used to examine the enrichment ability of the TiPCM. As shown in **Figures S3a–c**, there was no obvious difference between the three concentrations when they were used to enrich phosphopeptide. However, different results appeared for the enrichment of glycopeptide. When ACN/H_2O/TFA (79/20/1, v/v/v) was chosen to be the loading and washing solution, the glycopeptide signal was too weak, indicating that it is not suitable to use in enrichment (**Figure S3d**). When ACN/H_2O/TFA (79/18/3, v/v/v) and ACN/H_2O/TFA (79/16/5, v/v/v), respectively, were used to enrich glycopeptide, the number of non-glycopeptides decreased, and the glycopeptide signals grew stronger, as shown in **Figures S3e** and **S3f**. Because there was no significant

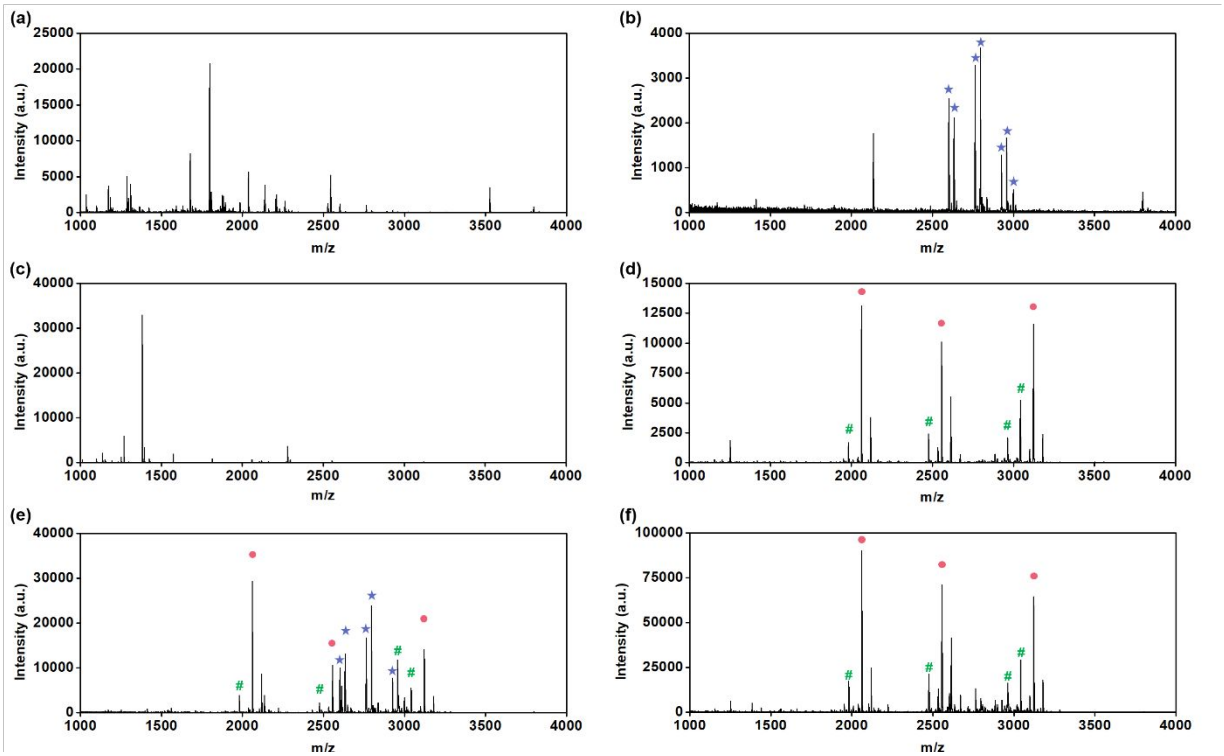

Figure 3 MALDI-TOF mass spectra of the tryptic digest of IgG after purified by SPE column. (a) Direct analysis and (b) analysis after enrichment by the TiPCM. MALDI-TOF mass spectra of the tryptic digest of β-casein after purified by SPE column. (c) Direct analysis and (d) analysis after enrichment by the TiPCM. MALDI-TOF mass spectra of the tryptic digest of IgG/β-casein mixture. (e) Simultaneous enrichment of phosphopeptides and glycopeptides and (f) enrichment of only phosphopeptides. Phosphopeptide peaks identified are marked with the symbol ●, dephosphorylated peptide peaks identified are marked with the symbol #, and glycopeptide peaks identified are marked with the symbol ★.

ARTICLE

Table 2 Comparison of enrichment performance of different materials for phosphopeptides and glycopeptides.

Material	Selectivity of phosphopeptide [a]	Selectivity of glycopeptide [b]	Limit of detecion (fmol)	Bifunctional	Reusable [c]	Ref.
Ti^{4+}-IMAC carbonaceous spheres	1/1000	/ [d]	5	No	/	36
$CuFeMnO_4$	1/100	/	20	No	/	37
Ti^{4+}-IMAC HPHMs	1/1000	/	5	No	/	38
Ti_3AlC_2	1/1000	/	5	No	Yes	39
SPMA	1/1000	/	10	No	/	40
Fe_3O_4-TiNbNS	1/38	/	16	No	/	41
N-wood & D-wood	/	1/345	10	No	/	42
PSDVB–PAM	/90	1/364	/	No	/	43
Glu-Schiff base@SiO_2	/	1/5000	/	No	/	44
BHCM	/	1/500	50	No	/	45
MoS_2/Au-NP–L-cysteine	/	1/1250	10	No	/	46
PNI-*co*-ATBA0.2@SiO_2	1/193	1/500	/	Yes	/	47
magOTfP5SOF-Ga^{3+}	1/385	1/1200	0.05	Yes	/	48
Ti^{4+}-immobilized MARs	1/77	1/10	1	Yes	/	49
TiPCM	1/5000	1/1000	5	Yes	Yes	This work

[a] β-casein/BSA (molar ratio); [b] IgG or HRP or fetuin/BSA (molar ratio); [c] For phosphopeptides enrichment; [d] The "/" means no mention in the article.

difference in the enrichment performance at the two conditions, the phosphopeptides should be eluted in a basic solution. Consequently, ACN/H_2O/TFA (79/18/3, v/v/v) was used to load and wash the phosphopeptides and glycopeptides, and 10% ammonia was used for elution, as shown in **Scheme 1b**.

As shown in **Figure 3a**, the glycopeptide signals were restrained due to the abundant non-glycopeptide signals. Consequently, only some glycopeptides could be detected when the unenriched and purified trypsin digests of IgG were directly analyzed using the MALDI-TOF system. After enrichment using the TiPCM, 33 glycopeptides could be detected, and the non-glycopeptide interference was almost completely eliminated, as can be seen in **Figure 3b** and **Table S1**. Similarly, as shown in **Figure 3c,** the phosphopeptides could be hardly detected when the unenriched and purified trypsin digests of β-casein was analysed because of the existence of non-phosphopeptide. However, all 3 phosphopeptides could be clearly detected after the trypsin digests of β-casein were enriched using the TiPCM. Meanwhile, 4 dephosphorylated peptides corresponding with the 3 phosphopeptides (**Figure 3d** and **Table S2**) could also be detected, and the non-phosphopeptide interference was almost completely eliminated. To evaluate the ability to simultaneously enrich both glycopeptides and phosphopeptides, a mixture of trypsin digests of IgG and β-casein (molar ratio, 10/1) was chosen for analysis. As shown in **Figure 3e** and **Table S3**, 30 glycopeptides, 3 phosphopeptides, and the corresponding 4 dephosphorylated peptides were detected, and the non-glycopeptide and non-phosphopeptide interferences were virtually eliminated. These results showed that the TiPCM possessed great potential for the simultaneous enrichment of both glycopeptides and phosphopeptides. Moreover, to use the TiPCM material to enrich target peptides (phosphopeptides), we investigated the individual enrichment ability for phosphopeptides from a mixture of trypsin digests of IgG and β-casein (molar ratio, 10/1) based on the process shown in **Scheme 1c**. As shown in the MALDI-TOF spectrum (**Figure 3f**), the signals of 3 phosphopeptides and the corresponding 4 dephosphorylated peptides appeared, the signals of several glycopeptides becoming very weak. Meanwhile, non-glycopeptide and non-phosphopeptid interferences were almost completely eliminated. These results showed that the TiPCM could be used to simultaneously enrich glycopeptides and phosphopeptides, as well as individually enrich phosphopeptides. The resulting materials exhibited high selectivity and flexible application potential in the enrichment of phosphopeptides and glycopeptides.

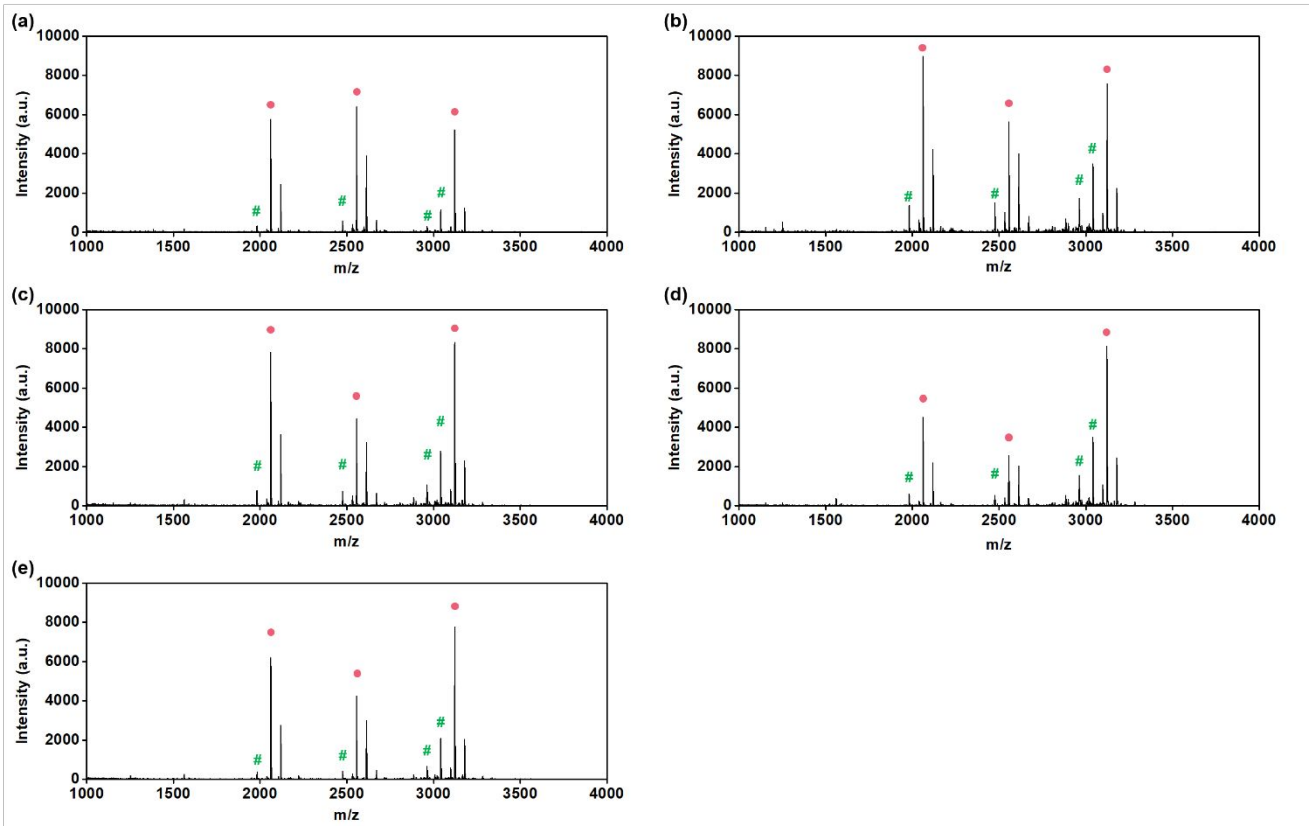

Figure 4 MALDI-TOF mass spectra of the tryptic digest of β-casein. The TiPCM was reused (a) 1st, (b) 2nd, (c) 3rd, (d) 4th, and (e) 5th times. The phosphopeptide peaks identified are marked with the symbol ●, and the dephosphorylated peptide peaks identified are marked with the symbol #.

To further evaluate the enrichment selectivity of the TiPCM, the phosphopeptides and glycopeptides were enriched from composite samples that the trypsin digests of BSA was combined with the trypsin digests of β-casein or IgG in different molar ratios, as shown in **Figures S4a–S4c**. When the TiPCM was used to enrich phosphopeptides from a 1/500 molar ratio of the tryptic digests of β-casein and BSA, the 3 phosphopeptides and their corresponding 4 dephosphorylated peptides were detected, and the non-phosphopeptide interferences were almost completely eliminated, as seen in **Figure S4a**. When the molar ratio of the β-casein to BSA trypsin digest was set to be 1/1000, the 3 phosphopeptides and their corresponding 4 dephosphorylated peptides could still be detected after enrichment by the TiPCM, the non-phosphopeptide signals could hardly be detected (**Figure S4b**). Most importantly, when the molar ratio was increased to 1/5000 (mass ratio of approximately 1/13000), all 3 phosphopeptides and their corresponding 4 dephosphorylated peptides were clearly detected despite the presence of a few non-phosphopeptide signals, as shown in **Figure S4c**. Moreover, the selectivity of the TiPCM for glycopeptide was also explored. It can be seen in **Figures S4d–S4f** and **Tables S4–S6**, that 26, 20, and 17 glycopeptides could be detected from the mixture of the tryptic digests of IgG and BSA at different molar ratios of 1/100, 1/500, and 1/1000, respectively.

Based on the low abundance of glycopeptide and phosphopeptide in the biological specimens tested, the detection sensitivity of the TiPCM was assessed, as shown in **Figure S5**. For the phosphopeptide enrichment, all 3 phosphopeptides could be detected from 50 fmol of trypsin digest of β-casein (**Figure S5a)**. When the content of the trypsin digest of β-casein was reduced to 5 fmol, all 3 phosphopeptides could still be observed (**Figure S5b)**. By contrast, the 23 glycopeptides could be enriched from 50 fmol of the trypsin digest of IgG, as shown in **Figure S5c** and **Table S7**. Moreover, when the content of the trypsin digest of IgG was decreased to 5 fmol, the 15 glycopeptides could still be detected (**Figure S5d** and **Table S8)**. The above results showed that the TiPCM material exhibited a high sensitivity for the enrichment of phosphopeptides and glycopeptides.

In **Table 2**, the selectivity and detection sensitivity of the TiPCM are compared with other reported materials for phosphopeptides and glycopeptides. As a result, the TiPCM exhibited excellent selectivity in phosphopeptide and glycopeptide enrichment, especially in phosphopeptides which was better than other reported materials used in phosphopeptide enrichment and the bifunctional materials used in phosphopeptide and glycopeptide enrichment. Meanwhile, **Table 2** can be used to compare the detection sensitivity of the TiPCM with other materials. It can be seen that its detection sensitivity exceeded the average level.

Furthermore, reusability is an important indicator for evaluating whether a material is suitably green and environmentally friendly. Generally, ammonia has been used to elute enriched

phosphopeptides from a material in the process of phosphopeptide enrichment, though the combination of Ti^{4+} and the material may be destroyed in alkaline conditions. Consequently, reusability has not been considered in most studies on phosphopeptide enrichment (as shown in **Table 2**). To verify that the TiPCM material is indeed environmentally friendly, we used 1 mg TiPCM to enrich phosphopeptides from 0.1 μg β-casein for 5 cycles. The results are shown in **Figure 4**. During 5 cycles, there was no obvious difference in the phosphopeptide enrichment results, demonstrating that the TiPCM possessed good reusability.

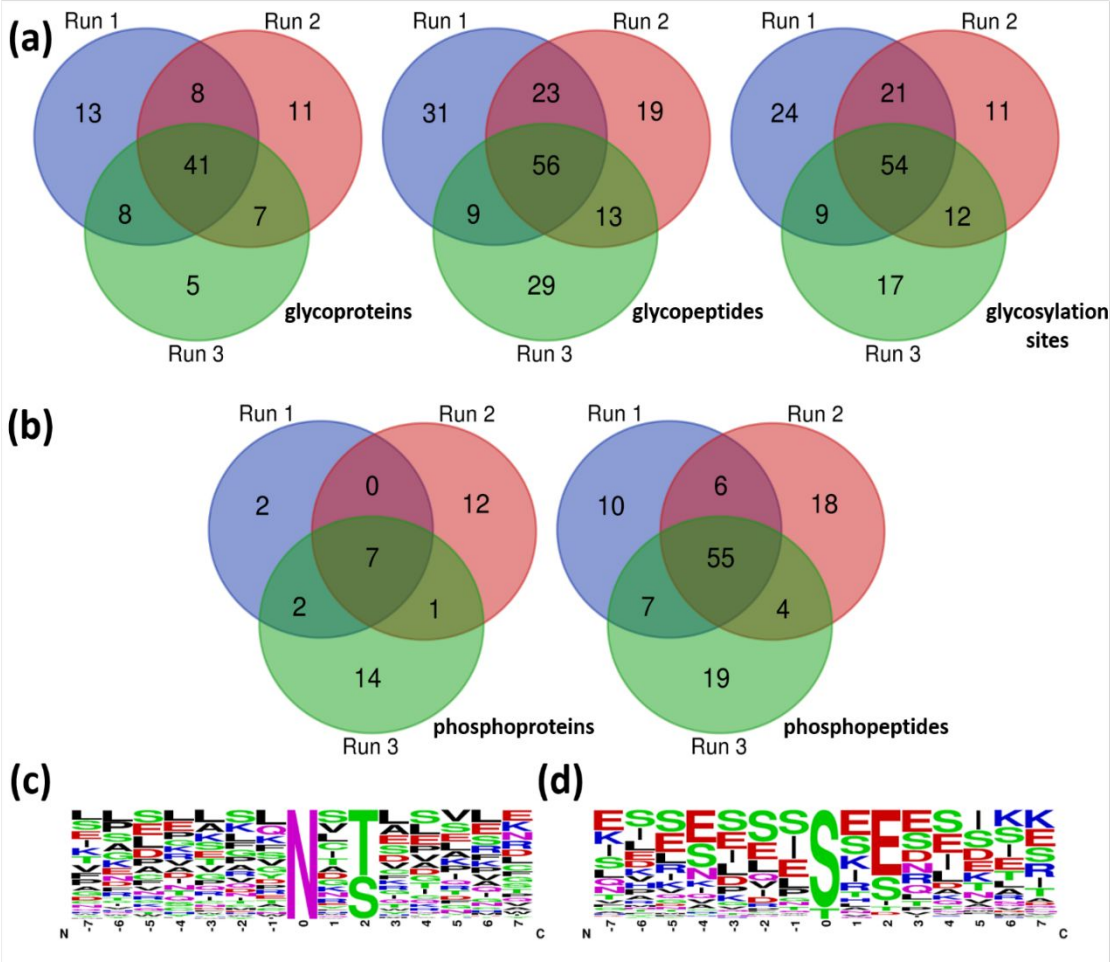

Figure 5 Identification results of the tryptic digest of milk after enrichment with the TiPCM via LC-MS/MS. (a) Venn diagrams of identified unique glycoproteins, glycopeptides, and glycosylation sites. (b) Venn diagrams of identified unique phosphoproteins and phosphopeptides. Motif analysis of (c) glycopeptides and (d) glycopeptides.

To further evaluate its phosphopeptide and glycopeptide enrichment ability, the tryptic digest of milk after enrichment with the TiPCM was analyzed via LC-MS/MS. Three parallel identifications were implemented based on **Scheme 1b**, the chromatogram (**Figures S6**) obtained being analyzed by database search. It could be found that 180 unique glycopeptides and the corresponding 148 glycosylation sites from 93 glycosylated proteins could be identified from the 3 parallel tests (**Figure 5a** and **Table S9**). Moreover, when 200 μg of the tryptic digest of milk enriched by the TiPCM was analyzed via LC-MS/MS, 119 unique phosphopeptides from 38 phosphorylated proteins could be identified from the 3 parallel tests (**Figure 5b** and **Table S10**). The motif composition of the identified glycosylation and phosphorylation sites are shown in **Figures 5c** and **5d**. The TiPCM exhibited promising potential for phosphopeptide and glycopeptide enrichment and is expected to be a green and efficient bifunctional material in the future.

Conclusions

In this study, green and inexpensive cellulose as precursor was utilized to prepare a hierarchically porous monolithic material (TiPCM) with a coral-like structure. The resulting TiPCM exhibited satisfactory hydrophilicity after the CM prepared *via* TIPS was phosphorylated, resulting in a large number of metal ion affinity sites to chelate Ti^{4+}. Moreover, the TiPCM possessed the ability to simultaneously enrich both phosphopeptides and glycopeptides. Its coral-like structure increased permeability to improve the mass transfer rate between the material and the enrichment solution, and greatly reduced steric effects between the peptide and the material. Moreover, its rough surface offered myriad adsorption sites during enrichment.

Consequently, the TiPCM showed excellent selective specificity and detection sensitivity for both phosphopeptides and glycopeptides. Compared with IMAC and HILIC materials with similar functions, preparation of the TiPCM was proved to be simple and green. Moreover, it could be reused to enrich phosphopeptides and flexibly enrich only phosphopeptides or both phosphopeptides and glycopeptides. It is expected to advance research on protein glycosylation and phosphorylation in the future.

Conflicts of interest

There are no conflicts to declare.

Acknowledgements

This work was supported by JSPS KAKENHI Grants (No. 19H02778, No. 20H02797), JST-Mirai Program (Grant No. JPMJMI18E3), and JOGMEC. L. Z. and Y. W. would like to thank China Scholarship Council (CSC) for a scholarship support.

References

1. P. Cohen, *Nature*, 1982, **296**, 613-620.
2. E. J. Nestler and P. Greengard., *Nature*, 1983, **305**, 583-588.
3. P. Cohen, *Nat. Cell Biol.*, 2002, **4**, E127–E130.
4. A. J. Whitmarsh and R. J. Davis., *Science*, 2016, **354**, 179-180.
5. A. S. Gajadhar, H. Johnson, R. J. Slebos, K. Shaddox, K. Wiles, M. K. Washington, A. J. Herline, D. A. Levine, D. C. Liebler and F. M. White, *Cancer Res.*, 2015, **75**, 1495-1503.
6. G. Giamas, Y. L. Man, H. Hirner, J. Bischof, K. Kramer, K. Khan, S. S. Ahmed, J. Stebbing and U. Knippschild, *Cell. Signal.*, 2010, **22**, 984-1002.
7. P. Cohen, *Eur. J. Biochem.*, 2001, **268**, 5001–5010.
8. Y. Jiang, A. Sun, Y. Zhao, W. Ying, H. Sun, X. Yang, B. Xing, W. Sun, L. Ren, B. Hu, C. Li, L. Zhang, G. Qin, M. Zhang, N. Chen, M. Zhang, Y. Huang, J. Zhou, Y. Zhao, M. Liu, X. Zhu, Y. Qiu, Y. Sun, C. Huang, M. Yan, M. Wang, W. Liu, F. Tian, H. Xu, J. Zhou, Z. Wu, T. Shi, W. Zhu, J. Qin, L. Xie, J. Fan, X. Qian and F. He, *Nature*, 2019, **567**, 257-261.
9. P. Blume-Jensen and T. Hunter., *Nature*, 2001, **411**, 355-365.
10. Y. Tian, Y. Zhou, S. Elliott, R. Aebersold and H. Zhang, *Nat. Protoc.*, 2007, **2**, 334-339.
11. A. Helenius and M. Aebi., *Science*, 2001, **291**, 2364-2369.
12. S. Hakomori, *Cancer Res.*, 1985, **45**, 2405-2414.
13. H. H. Freeze, *J. Biol. Chem.*, 2013, **288**, 6936-6945.
14. C. A. Reis, H. Osorio, L. Silva, C. Gomes and L. David, *J. Clin. Pathol.*, 2010, **63**, 322-329.
15. S. S. Pinho and C. A. Reis, *Nat. Rev. Cancer*, 2015, **15**, 540-555.
16. T. Cell Press Editorial, *Cell*, 2020, **180**, 1.
17. S. Kumar, V. K. Maurya, A. K. Prasad, M. L. B. Bhatt and S. K. Saxena, *Virusdisease*, 2020, **31**, 13-21.
18. G. Durand and N. Seta., *Clin. Chem.*, 2000, **46**, 795–805.
19. T. M. Block, M. A. Comunale, M. Lowman, L. F. Steel, P. R. Romano, C. Fimmel, B. C. Tennant, W. T. London, A. A. Evans, B. S. Blumberg, R. A. Dwek, T. S. Mattu and A. S. Mehta., *Proc. Natl. Acad. Sci. U. S. A.*, 2005, **102**, 779-784.
20. A. Leitner, *Trends Anal. Chem.*, 2010, **29**, 177-185.
21. Matthew P. Stokes, Charles L. Farnsworth, Albrecht Moritz, Jeffrey C. Silva, Xiaoying Jia, Kimberly A. Lee, Ailan Guo, Roberto D. Polakiewicz and M. J. Comb., *Mol. Cell. Proteomics*, 2012, **11**, 187–201.
22. H. Zhou, M. Ye, J. Dong, E. Corradini, A. Cristobal, A. J. Heck, H. Zou and S. Mohammed, *Nat. Protoc.*, 2013, **8**, 461-480.
23. Y. Hu, B. Jiang, Y. Weng, Z. Sui, B. Zhao, Y. Chen, L. Liu, Q. Wu, Z. Liang, L. Zhang and Y. Zhang, *Nat. Commun.*, 2020, **11**, 6226.
24. J. Porath, *Trends Anal. Chem.*, 1988, **7**, 254-259.
25. H. Zhang, X. J. Li, D. B. Martin and R. Aebersold, *Nat. Biotechnol.*, 2003, **21**, 660-666.
26. S. Mysling, G. Palmisano, P. Højrup and M. Thaysen-Andersen., *Anal. Chem.*, 2010, **82**, 5598-5609.
27. G. Qing, J. Yan, X. He, X. Li and X. Liang, *TrAC, Trends Anal. Chem.*, 2020, **124**, 115570.
28. P. Gallezot, *Chem. Soc. Rev.*, 2012, **41**, 1538-1558.
29. Z. T. Xie, T. A. Asoh, Y. Uetake, H. Sakurai and H. Uyama, *Carbohydr. Polym.*, 2020, **247**, 116723.
30. S. Mizuno, T. A. Asoh, Y. Takashima, A. Harada and H. Uyama, *Chem. Commun.*, 2020, **56**, 14408-14411.
31. Y. Xin, Q. Xiong, Q. Bai, M. Miyamoto, C. Li, Y. Shen and H. Uyama, *Carbohydr. Polym.*, 2017, **157**, 429-437.
32. Y. Huang and Y. Fu, *Green Chem.*, 2013, **15**, 1095.
33. D. Huang, F. Benzoni, H. Fukami, N. Knowlton, N. D. Smith and A. F. Budd, *Zool. J. Linn. Soc.*, 2014, **171**, 277-355.
34. B. G. Fiss, L. Hatherly, R. S. Stein, T. Friščić and A. Moores, *ACS Sustainable Chem. Eng.*, 2019, **7**, 7951-7959.
35. Z. Xiong, Y. Chen, L. Zhang, J. Ren, Q. Zhang, M. Ye, W. Zhang and H. Zou, *ACS applied materials & interfaces*, 2014, **6**, 22743-22750.
36. H. Zhang, X. Li, S. Ma, J. Ou, Y. Wei and M. Ye, *Green Chem.*, 2019, **21**, 2052-2060.
37. X. Y. Long, Z. J. Zhang, J. Y. Li, D. Sheng and H. Z. Lian, *Anal. Chem.*, 2017, **89**, 10446-10453.
38. H. Zhang, J. Ou, Y. Yao, H. Wang, Z. Liu, Y. Wei and M. Ye, *Anal. Chem.*, 2017, **89**, 4655-4662.
39. X. Li, N. Zhang, R. Tang, J. Lyu, Z. Liu, S. Ma, J. Ou and M. Ye, *Nanoscale*, 2021, **13**, 2923-2930.
40. B. Luo, M. Yang, P. Jiang, F. Lan and Y. Wu, *Nanoscale*, 2018, **10**, 8391-8396.
41. X. Chen, S. Li, X. Zhang, Q. Min and J. J. Zhu, *Nanoscale*, 2015, **7**, 5815-5825.
42. Y. Zhou, X. Sheng, J. Garemark, L. Josefsson, L. Sun, Y. Li and Å. Emmer, *Green Chem.*, 2020, **22**, 5666-5676.
43. Y. Song, X. Li, J. B. Fan, H. Kang, X. Zhang, C. Chen, X. Liang and S. Wang, *Adv. Mater.*, 2018, **30**, e1803299.
44. Y. Xiong, X. Li, M. Li, H. Qin, C. Chen, D. Wang, X. Wang, X. Zheng, Y. Liu, X. Liang and G. Qing, *J. Am. Chem. Soc.*, 2020, **142**, 7627-7637.
45. L. Zhang, S. Ma, Y. Chen, Y. Wang, J. Ou, H. Uyama and M. Ye, *Anal. Chem.*, 2019, **91**, 2985-2993.
46. C. Xia, F. Jiao, F. Gao, H. Wang, Y. Lv, Y. Shen, Y. Zhang and X. Qian, *Anal. Chem.*, 2018, **90**, 6651-6659.
47. Q. Lu, C. Chen, Y. Xiong, G. Li, X. Zhang, Y. Zhang, D. Wang, Z. Zhu, X. Li, G. Qing, T. Sun and X. Liang, *Anal. Chem.*, 2020, **92**, 6269-6277.
48. H. Zheng, J. Jia, Z. Li and Q. Jia, *Anal. Chem.*, 2020, **92**, 2680-2689.
49. R. Tang, Y. Yu, J. Dong, Y. Yao, S. Ma, J. Ou and M. Ye, *Anal. Chim. Acta*, 2021, **1144**, 111-120.